A Temperature-sensitive *NUP116* Null Mutant Forms a Nuclear Envelope Seal over the Yeast Nuclear Pore Complex Thereby Blocking Nucleocytoplasmic Traffic

Susan R. Wente and Günter Blobel

Laboratory of Cell Biology, Howard Hughes Medical Institute, The Rockefeller University, New York 10021

Abstract. *NUP116* encodes a 116-kD yeast nuclear pore complex (NPC) protein that is not essential but its deletion (*nup116Δ*) slows cell growth at 23°C and is lethal at 37°C (Wente, S. R., M. P. Rout, and G. Blobel. 1992. *J. Cell Biol.* 119:705–723). Electron microscopic analysis of *nup116Δ* cells shifted to growth at 37°C revealed striking perturbations of the nuclear envelope: a double membrane seal that was continuous with the inner and outer nuclear membranes had formed over the cytoplasmic face of the NPCs. Electron-dense material was observed accumulating between the cytoplasmic face of these NPCs and the membrane seal, resulting in "herniations" of the nuclear envelope around individual NPCs. In situ hybridization with poly(dT) probes showed the accumulation of polyadenylated RNA in the nuclei of arrested *nup116Δ* cells, sometimes in the form of punctate patches at the nuclear periphery. This is consistent with the electron microscopically observed accumulation of electron-dense material within the nuclear envelope herniations. We propose that *nup116Δ* NPCs remain competent for export, but that the formation of the membrane seals over the NPCs blocks nucleocytoplasmic traffic.

THE nuclear pore is a circular opening of ~90 nm diameter that traverses the double membrane of the nuclear envelope (Franke et al., 1981). This pore is presumably formed by a circumscribed fusion of the outer and inner nuclear membranes. Throughout cellular division and differentiation, the number of nuclear pores per nucleus has been found to not only increase, but also to decrease (reviewed in Maul, 1977). Therefore, membrane fusion may also be required for the elimination of a nuclear pore and restoration of an uninterrupted double membrane structure. However, the mechanism by which either of these fusion events occurs has not been elucidated.

The nuclear pore is occupied by the nuclear pore complex (NPC),[1] a modular structure of an estimated molecular mass of ~10^8 D that mediates the bidirectional transport of macromolecules between the nucleus and the cytoplasm (for review see Forbes, 1992). Based upon this mass (Reichelt et al., 1990), the NPC is estimated to be comprised of a hundred or more distinct polypeptides. Only a few of these proteins, referred to collectively as nucleoporins (Davis and Blobel, 1986), have been molecularly characterized in yeast and other eukaryotic cells (Starr et al., 1990; Davis and Fink, 1990; Nehrbass et al., 1990; Wente et al., 1992; Wimmer et al., 1992; Sukegawa and Blobel, 1993; Loeb et al., 1993; Radu et al., 1993). The sublocalization of these nucleoporins to the distinct structures of an NPC (i.e., rings, spokes, plug, fibers, cages) (Akey, 1992) has not been accomplished. It is also not known how these modular structures are formed and reversibly assembled into a functional NPC. Vesicular and soluble components have both been found to be necessary for the in vitro assembly of transport competent NPCs from fractionated frog egg extracts (Sheehan et al., 1988; Finlay and Forbes, 1990; Dabauvalle et al., 1990; Finlay et al., 1991; Vigers and Lohka, 1991).

The anchorage of the assembled NPC to the nuclear pore is presumably mediated by integral membrane proteins that are specifically localized to the membrane surrounding the NPC. Because of its distinct protein composition, this region of the nuclear envelope is referred to as the pore membrane (Hallberg et al., 1993). Three distinct, integral pore membrane proteins have so far been molecularly characterized: gp210 (Gerace et al., 1982; Wozniak et al., 1989) and POM121 (Hallberg et al., 1993) both of rat, and POM152 of yeast (Wozniak, R., G. Blobel, and M. P. Rout, personal communication). It has not been determined which of the pore membrane proteins serve as anchors for the NPC.

In this paper we report the characterization of a mutant yeast strain with a chromosomal deletion of the gene encoding NUP116, a member of a family of nucleoporins that share an amino terminal domain of repetitive tetrapeptide "GLFG" motifs (Wente et al., 1992). At 23°C, the *NUP116* null (*nup116Δ*) cells grow slower than wild-type cells and the

Dr. Wente's present address is Department of Cell Biology and Physiology, Washington University School of Medicine, St. Louis, MO 63110.

1. *Abbreviations used in this paper*: HA, epitope tag from the influenza hemagglutinin antigen; NPC, nuclear pore complex.

Table I. Yeast Strain Genotype and Construction

Strain	Genotype	Derivation
W303a	Mata ade2-1 ura3-1 his3-11,15 trp1-1 leu2-3,112 can1-100	
W303α	Matα ade2-1 ura3-1 his3-11,15 trp1-1 leu2-3,112 can1-100	
CG-D	Mata/Matα ade5/ade5 can1^r/+ his7-2/+ leu2-3,112/leu2-3,112 trp1-289/trp1-289 ura3-52/ura3-52	Cross of CG378^a and CG379$^\alpha$ from Bruschi et al., 1987
SWY26	Mata/Matα ade2-1/ade2-1 ura3-1/ura3-1 his3-11,15/his3-11,15 trp1-1/trp1-1 leu2-3,112/leu2-3,112 can1-100/can1-100 nup116-5::HIS3/+	Wente et al., 1992
SWY27	Matα ade2-1 ura3-1 his3-11,15 trp1-1 leu2-3,112 can1-100 nup116-5::HIS3	Segregant from tetrad of sporulated SWY26
SWY29	Mata ade2-1 ura3-1 his3-11,15 trp1-1 leu2-3,112 can1-100 nup116-5::HIS3	Wente et al., 1992
SWY31	Matα ade2-1 ura3-1 his3-11,15 trp1-1 leu2-3,112 can1-100 nup116-6::URA3	Wente et al., 1992
SWY55	Mata ade2-1 ura3-1 his3-11,15 trp1-1 leu2-3,112 can1-100 nup116-6::URA3 pSW76(LEU2)	Wente et al., 1992
SWY59	Mata/Matα ade2-1/ade2-1 ura3-1/ura3-1 his3-11,15/his3-11,15 trp1-1/trp1-1 leu2-3,112/leu2-3,112 can1-100/can1-100 nup116-6::URA3/nup116-5::HIS3	Cross of SWY29 and SWY31
SWY61	Matα ade2-1 ura3-1 his3-11,15 trp1-1 leu2-3,112 can1-100 nup116-5::HIS3	Segregant from tetrad of sporulated diploid from a SWY27 X W303a cross
SWY117	Mata/Matα ade5/ade5 can1^r/+ his7-2/+ leu2-3,112/leu2-3,112 trp1-289/trp1-289 ura3-52/ura3-52 nup116-6::URA3/+	Integrative transformation of CG-D with EcoRI fragments of pSW54
SWY118	Mata ade5 can1 his7-2 leu2-3,112 trp1-289 ura3-52 nup116-6::URA3	Segregant from tetrad of sporulated SWY117
SWY138	Matα ade2-1 ura3-1 his3-11,15 trp1-1 leu2-3,112 can1-100 pSW134(URA3)	Transformation of W303α with pSW134

Yeast transformations were by the lithium acetate method (Ito et al., 1983) and general genetic manipulations were conducted as described by Sherman et al. (1986).

only observed ultrastructural changes are the occurrence of invaginations of the inner nuclear membrane that are studded with densities similar in size to NPCs. At 37°C, *nup116Δ* cells cease growing. Electron microscopic examination reveals that the mutant NPCs still appear to be in place and to be membrane anchored. However, a double membrane seal continuous with the inner and outer nuclear membranes, respectively, had formed over the cytoplasmic face of the NPCs. This "sealing off" of the NPCs prevents nucleocytoplasmic trafficking.

Materials and Methods

Yeast Strains and Plasmids

The yeast strains that were used in this study are described in Table I. The W303 strains were provided by Dr. R. Rothstein. To ascertain that our experimental observations are not due to an artifact in the original strain background or to an accumulation of suppressors in the *NUP116* null (*nup116Δ*) strain, several precautions have been taken. First, the *nup116Δ* strain (SWY27) was backcrossed against the wild-type parent strain (W303a) and, after sporulation of the resulting heterozygous diploid, dissected to yield haploid *nup116Δ* daughter cells (SWY61). Second, the null deletion was made in a different strain background (SWY118), and finally, a diploid null strain was also constructed and similarly analyzed (SWY59). All of the null strains (SWY27, SWY61, SWY118, SWY59) regardless of their genetic background display identical growth phenotypes and the morphological perturbations described in this paper.

The plasmids pSW54, pSW72, pSW75, and pSW76 are described in Wente et al. (1992), and pLGSD5 is from Guarente et al., (1982). The construction of the plasmid pSW134 was conducted using the general DNA manipulations described by Sambrook et al. (1989). A unique BglII site was inserted just before nucleotide No. 731 (amino acid No. 2) and a unique SacI site was inserted in the 3′ untranslated region, just after bp 422, in the sequence for *NUP116* (pSW72) by the polymerase chain reaction with appropriate oligonucleotides. The resulting 3,500-bp BglII–SacI fragment was ligated into the BamHI–SacI digested vector from pLGSD5 (2 μm, *URA3*), thus fusing the coding sequence for *NUP116* (minus the initiation codon) in frame with the second amino acid of the *CYC1* gene under control of the *GAL10* promoter. Enzymes were obtained from either New England Biolabs, Inc. (Beverly, MA) or Perkin Elmer Cetus (Norwalk, CT).

Cell Growth and Analysis

The yeast strains were grown in rich media (YPD, 1% yeast extract, 2% bactopeptone, 2% glucose) or synthetic minimal media (SM; Sherman et al., 1986) supplemented with appropriate amino acids and a final concentration of either 2% glucose or 2% galactose (plus 2% agar for growth on plates). Where indicated, filter sterilized cycloheximide (Sigma Chemical Co., St. Louis, MO) was added to YPD liquid cultures at a final concentration of 100 μg/ml.

The photomicroscopic analysis of yeast cells was performed by fixing a pelleted aliquot of 10^8 cells from an early logarithmic phase culture in buffer A (40 mM K_2HPO_4-KH_2PO_4, pH 6.5, 0.5 mM $MgCl_2$) containing 3.7% formaldehyde (Fluka Chemical Corp., Ronkonkoma, NY) for 2 h at room temperature. The fixed cells were pelleted (1,000 *g*), resuspended in buffer A, centrifuged again, and after final resuspension in buffer A briefly sonicated and spotted on polylysine-coated coverslips. The attached cells were dehydrated by incubating the slide first in ice cold methanol for 5 min, and then 30 s in room temperature acetone. The cell-coated coverslips were briefly washed with buffer A and then mounted with 90% glycerol, 1 mg/ml *p*-phenylenediamine, 0.05 μg/ml DAPI at pH 8.0. Photographs were taken with the 40× objective on a Zeiss Axiophot microscope with Kodak T-MAX 400 film processed at 1600 ASA (Eastman Kodak Co., Rochester, NY).

Total yeast cell extracts were made as described by Yaffe and Schatz (1984). Nitrocellulose blots from the electrophoretic transfer of proteins in polyacrylamide gels were incubated overnight at 4°C with a 1:5 dilution of the respective mAb tissue culture supernant in TBST buffer (10 mM Tris-HCl, pH 8.0, 150 mM NaCl, 0.1% Tween-20) plus 2% nonfat dry milk. With TBST buffer washes between, sequential incubations with affinity purified anti-mouse IgG (Cappel Laboratories, Organon Teknika Corp., West Chester, PA) (diluted 1:500 in TBST, 1 h at room temperature [RT]) and then ^{125}I-protein A (100 μCi/ml; Dupont NEN, Wilmington, DE) (diluted 1:200 in TBST, 1 h, RT) were conducted. The processed blots were dried and exposed for autoradiography.

Immunoelectron Microscopy

The immunolocalization of epitope tagged NUP116 was performed as previ-

ously described by Wente et al., (1992) except the samples were embedded in Lowicryl. The thin sections from postembedded spheroplasts of SWY55 were incubated with undiluted tissue culture supernant of the mAb 12CA5 (Berkeley Antibody Co., Richmond, CA), and 10-nm colloidal gold coated with goat anti-mouse antibody (Amersham Corp., Arlington Heights, IL).

For the immunoelectron microscopy localization of nucleoporins in the temperature arrested *nup116Δ* cells a different protocol was used. A culture of SWY27 was grown at 23°C to early logarithmic phase and then shifted for 3 h at 37°C. An aliquot of 10^8 cells was removed and formaldehyde (37% stock; Fluka Chemical Corp.) was immediately added to a final concentration of 4%. After 5 min at room temperature, the fixed cells were washed by a cycle of centrifugation (1,000 *g*) and resuspension in buffer A. The cells were resuspended in a final volume of 1.5 ml fixative (4% formaldehyde, 0.075% glutaraldehyde [25% stock; BDH, Gallard Schlesinger Chem., Carle Place, NY], 40 mM K_2HPO_4-KH_2PO_4, pH 6.5, 0.5 mM $MgCl_2$) and incubated on ice for 1 h. The fixed cells were washed into 0.1 M phosphate-citrate buffer (Byers and Goetsch, 1991) by two cycles of centrifugation (1,000 *g*) and resuspension in this buffer, and then resuspended in 0.5 ml of the 0.1 M phosphate-citrate buffer plus a 1/10 dilution of Glusulase (Dupont NEN), 0.1 mg/ml Zymolyase 20T (Seikagaku Corp., Tokyo, Japan), and 0.1 mg/ml Mutanase (Novo Nordisk Bioindustrials, Inc., Danbury, CT). After incubation for 2 h at 30°C, the pellets were washed, dehydrated, and embedded in Lowicryl. Thin sections were collected and processed for immunolocalization with a 1:1 mixture of the tissue culture supernants for MAb192 and MAb350 as previously described (Wente et al., 1992).

Specimens were visualized with a JEOL 100CX electron microscope (JEOL USA, Inc., Peabody, MA) at 80 kV, and photographs were recorded with Kodak electron microscopy film (Eastman Kodak Co.).

Electron Microscopy for Ultrastructural Morphology

A variety of fixation conditions, embedding media, and staining methods were examined, and the protocols were selected solely on the basis of optimized visualization primarily of proteins, or of membranes, or of proteins and membranes at the nuclear envelope. The cells (SWY27 and W303α) that were grown to early logarithmic phase before shifting to the indicated growth temperatures (for defined times) were immediately fixed by resuspension of the cell pellet in buffer A containing 2% glutaraldehyde, 2% formaldehyde, and incubation for 30 min on ice. The cell wall was then removed in the same manner as described above for immunoelectron microscopy. The visualization primarily of the proteins associated with the nuclear envelope was achieved by using the osmium postfixation and Spurrs embedding procedures of Byers and Goetsch (1991) for vegetatively grown cells (see Figs. 3 and 4 *A*). Preservation of both protein and membrane structures was obtained by following the above protocol and embedding in Epon instead of Spurrs resin (see Figs. 4, *B*, *D*, and *E*, and 8). Finally, an osmium tetroxide-ferrocyanide postfixation protocol coupled with embedding in Spurrs resin (Wright et al., 1988) was used for the samples that preferentially visualized the nuclear membrane (see Fig. 4 *C*).

In situ Hybridization for Polyadenylated RNA Localization

Early logarithmic phase cultures of wild-type (W303α) and *nup116Δ* (SWY27) cells were grown at 23°C before shifting to 37°C. Aliquots of 10^8 cells were removed at time intervals after the temperature shift and formaldehyde was added to a final concentration of 4%. The cells were immediately pelleted, washed, and then resuspended in a fixative of 3.7% formaldehyde, 10% methanol, 0.1 M potassium phosphate, pH 6.5 for 1 h at room temperature. Cell wall removal from the fixed cells was described above for the immunoelectron microscopy samples. After spotting the processed cells on polylysine-coated coverslips, they were dehydrated by incubating the coverslip in ice-cold methanol for 6 min, and then in room temperature acetone for 30 s. The cell-coated coverslips were rinsed with 2× SSC (0.3 M NaCl, 30 mM sodium citrate, pH 7), and the subsequent in situ hybridization and immunolocalization steps were conducted exactly as described by Forrester et al. (1992). The oligonucleotide poly$(dT)_{30}$ probe was end labeled by terminal transferase (GIBCO BRL, Gaithersburg, MD) with digoxigenin-11-dUTP (Boehringer Mannheim, Mannheim, Germany) (Amberg et al., 1992). Anti-digoxigenin-fluorescein fAb fragments were obtained from Boehringer Mannheim. Photographs were taken with the 100× objective on a Zeiss Axiophot microscope for the same exposure time with Kodak T-MAX 400 film (Eastman Kodak Co.), and processed at 1600 ASA.

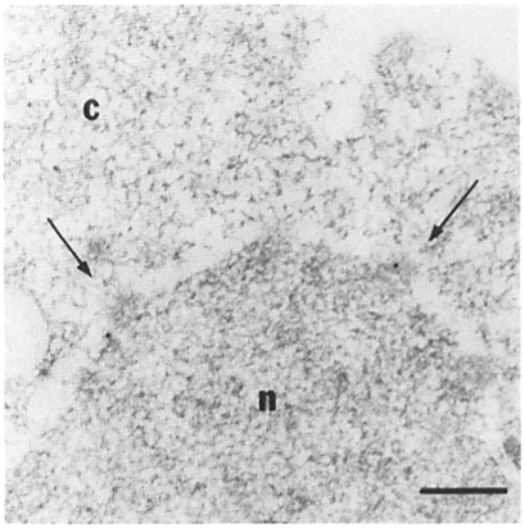

Figure 1. Epitope-tagged NUP116 is localized at the yeast nuclear pore complexes. Immunolabeling of thin sections from Lowicryl-embedded yeast spheroplasts of the haploid strain SWY55 (HA-tagged NUP116) was performed as described in Materials and Methods. The binding of the mAb (12CA5) which recognizes the epitope tag was visualized by colloidal gold particles (10 nm) coated with a goat anti-mouse antibody. In the micrograph, the nucleoplasm (*n*) and cytoplasm (*c*) are separated by a clear area between the nuclear membranes. The NPCs appear as protein dense patches along the nuclear envelope, and the gold particles that label such NPCs are indicated by arrows. Quantitation of the gold particles in representative cell thin sections is presented in Table II. Bar, 0.2 μm.

Results

NUP116 Is a Nuclear Pore Complex Protein

We have previously reported the isolation of the gene *NUP116* from *Saccharomyces cerevisiae* that encodes a 116-kD polypeptide with sequence similarities and subcellular fractionation properties common to other yeast nucleoporins (Wente et al., 1992). Localization of NUP116 was achieved by inserting in the gene the sequence encoding a unique nine-amino acid epitope derived from the influenza hemagglutinin antigen (HA), and then expressing this tagged construct in the null strain background (*nup116-3::HA*, SWY55). Indirect immunofluorescence using a mAb (12CA5) directed against the HA epitope revealed punctate, nuclear rim staining consistent with localization to the NPC (Wente et al., 1992). To definitively localize NUP116 to the NPC we have performed immunoelectron microscopy with thin sections from postembedded spheroplasts of the strain expressing the epitope-tagged *NUP116*. As shown in Fig. 1, NUP116 was found along the nuclear envelope and coincident with protein densities typical of NPCs. Quantitation data for total gold particle localization are shown in Table II and are similar to that previously reported for the HA-tagged NUP49 (Wente et al., 1992). This confirms the identification of NUP116 as a yeast nucleoporin.

nup116Δ Cells Are Not Viable at 37°C

Our previous studies indicated that *NUP116*, while not essential, was important for cell growth (Wente et al., 1992).

Table II. Distribution of Antibody Labeling in Immunoelectron Microscopy Experiments

Location	Number of gold particles	Density (*gold particles/μm²*)
A. 12CA5 antibody localization of epitope-tagged NUP116		
Nucleoplasm	3	0.2
NPC/NE	38	5.1
Cytoplasm	17	0.2
B. MAb192/MAb350 localization in arrested *nup116Δ* cells		
Nucleoplasm	6	
Interior of Herniation	1	
Base of Herniation	36	
NPC/NE	21	
Cytoplasm	12	

The number and location of 10-nm gold particles in 12 typical thin sections for the immunoelectron microscopy experiments in Figs. 1 and 5 are shown in *A* and *B*, respectively. In *B*, only cell sections that contained nuclear envelope herniations were used. The density of gold particles in *A* was calculated using the average area of the nucleoplasm, nuclear envelope (*NE*), and cytoplasm from representative sections of five cells.

Haploid *NUP116* null strains (*nup116Δ*) are viable although slow growing. In rich media at 23°C, *nup116Δ* strains have doubling times of nearly 6 h, at least three times longer than wild-type strains. Microscopic examination of wild-type and *nup116Δ* cells revealed that the mutant cells were somewhat larger (data not shown). As the mutant was generated by the deletion of a nucleoporin, we examined the ultrastructure of the nuclear envelope and NPCs by EM. The only noticeable structural aberrations in *nup116Δ* cells grown at 23°C are invaginations of the inner nuclear membrane (data not shown, see below in Fig. 4).

Because we found both morphological and growth differences in the *nup116Δ* cells as compared to wild type when grown at 23°C, we tested the *nup116Δ* cells for their ability to grow at a range of temperatures above and below 23°C (permissive temperature). The *nup116Δ* cells do not appear to be cold sensitive as they are viable when grown at 17°C, and there is no measurable change in the ratio of mutant to wild-type growth rates as compared to 23°C. However, whereas the *nup116Δ* mutant strains grow at 23°C (Fig. 2 *A*, *upper panel*), they do not grow at 37°C (nonpermissive temperature, Fig. 2 *A*, lower panel). Cell doubling ceases after at most one cellular division, and mutant cells shifted to 37°C become progressively inviable with time; such that after 8 h <15% are viable cells when returned to the permis-

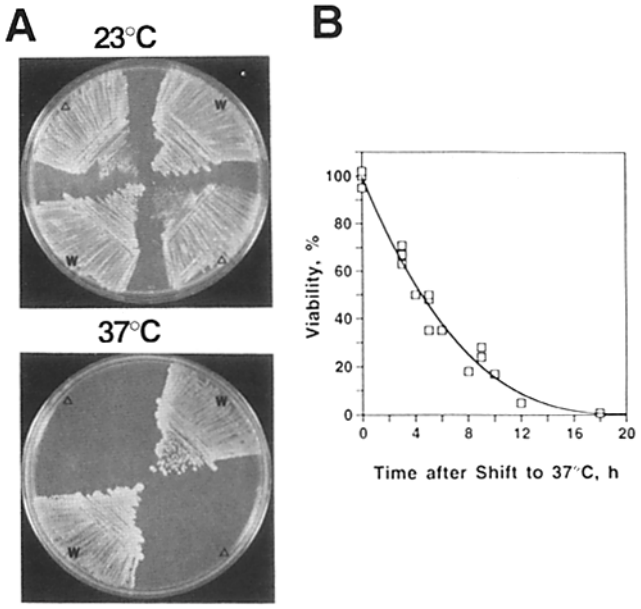

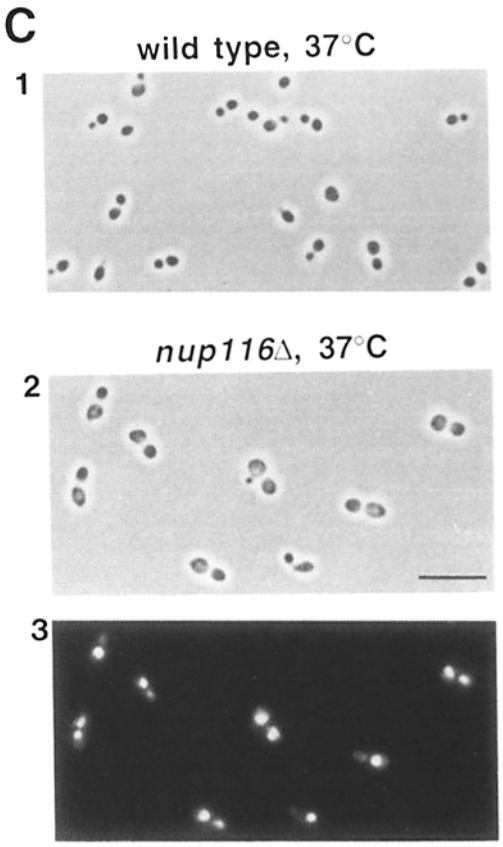

Figure 2. The temperature sensitive growth phenotype of *NUP116* deletion. (*A*) Deletion of *NUP116* results in a temperature sensitive lethal strain at 37°C. Cells isolated from each single tetrad of a sporulated diploid heterozygous for the *nup116Δ* allele (SWY26) were streaked on YPD plates. The upper plate was incubated for 5 d at 23°C, the lower at 37°C for 3 d. The *nup116Δ* strains (designated Δ), SWY27 and SWY29, were shown by Southern analysis and immunoblotting to lack the *NUP116* gene and protein, respectively. The strains designated w were wild type by the same criteria. (*B*) Viability of *nup116Δ* cells after growth at nonpermissive temperature (37°C) decreases sharply. At time zero, an early logarithmic phase culture of SWY27 (from 23°C growth in rich media) was shifted to 37°C and aliquots were removed at the indicated time points, plated on YPD plates, incubated at 23°C, and the number of viable colonies scored. (*C*) Morphology of *nup116Δ* cells is distinct from wild-type cells. The photographs are representative fields of cells from logarithmic phase cultures of wild-type or *nup116Δ* haploid strains (W303α and SWY27, respectively) that were grown at 23°C in rich media, shifted to 37°C for 3 h, fixed, and processed as described in Materials and Methods. *C 3* shows the coincident DAPI staining for the respective field of *nup116Δ* cells in *C 2*. All photographs were taken with a 40× objective (with Nomarski optics for *C*, *1* and *2*). Bar, 20 μm.

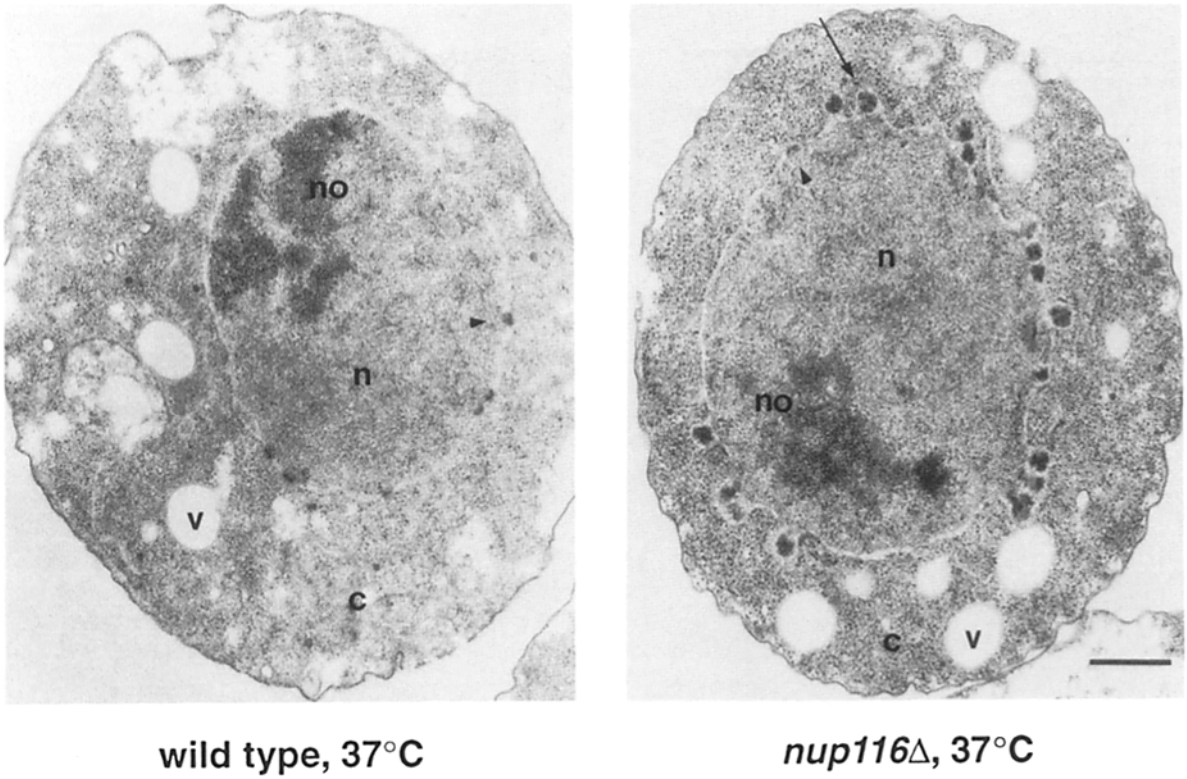

Figure 3. Thin-section electron micrographs of wild-type and *nupl16Δ* cells grown at 37°C. The wild-type (W303α) and *nupl16Δ* (SWY27) cells were grown to early logarithmic phase at 23°C in rich media before shifting to growth at 37°C for 3 h, and then processing for optimal visualization of protein structures (see Materials and Methods). The arrowheads in both micrographs point to representative nuclear pore complexes embedded in the nuclear envelope. The striking difference between the wild-type and mutant cells is the presence of nuclear envelope associated, electron dense material (i.e., at arrow). The large electron-dense structures are not present when the *nupl16Δ* cells are grown at the permissive temperature (data not shown). *no*, nucleolus; *n*, nucleus; *c*, cytoplasm; *v*, vacuole; Bar, 0.5 μm.

sive temperature (Fig. 2 *B*). The *nupl16Δ* cells grown at the permissive or nonpermissive temperature exhibit no measurable change in the relative amounts of any of the other GLFG nucleoporins as compared with wild-type cells (as judged by immunoblots of whole cell extracts, data not shown). The temperature-sensitive phenotype can be complemented by transformation of the *nupl16Δ* strain with plasmids bearing wild-type or epitope-tagged *NUPl16* (data not shown).

Besides the terminal lethal phenotype, the gross cellular morphology of *nupl16Δ* cells grown at the nonpermissive temperature is distinct from that of wild-type cells. *nupl16Δ* cells grown for 3 h at 37°C are significantly larger (Fig. 2 *C*, *2*) than similarly grown wild-type cells (Fig. 2 *C*, *1*). Under these conditions, the mutant cells are still 75% viable if shifted back to the permissive temperature (see Fig. 2 *B*). Growth at 37°C also markedly increases the proportion of large budded cells to at least 85% of the mutant cell population (Fig. 2 *C*, *2*). Furthermore, the panel in Fig. 2 *C*, *3* shows that in most of the arrested cells the nucleus is extended into the bud.

Herniations of Nuclear Envelope Over Nuclear Pore Complexes

Electron microscopy of wild-type yeast cells at 37°C shows the presence of typical NPCs embedded in the nuclear envelope (Fig. 3, *left panel*, *arrowhead*). However, in *nupl16Δ* cells grown for 3 h at 37°C, large electron-dense structures are observed at the perimeter of the nucleus (Fig. 3, *right panel*, *arrow*). A more detailed electron microscopic analysis is shown in Fig. 4. *nupl16Δ* cells were grown either for 3 h (Fig. 4, *A–D*) or for 9 h (*E*) at 37°C. The cells were processed under a variety of conditions (see Materials and Methods) for either optimized visualization of protein (Fig. 4 *A*), membranes (*C*), or protein as well as membranes (*B*, *D*, and *E*). The electron-dense material at the nuclear perimeter (Fig. 4, *A*, *B*, *D*, and *E*) appears to be enclosed by herniations of the inner and outer nuclear membranes (*B*, *C*, *D*, and *E*). At the nucleoplasmic base of these herniations, electron dense structures resembling NPCs (Fig. 4, *A*, *B*, *D*, and *E*) are present and seem to be anchored to the membrane (for example see panel *D* at 1 o'clock).

Several individual herniations of the inner membrane may be enclosed by a single large outer membrane herniation (Fig. 4, *B* and *E*). The size of the individual herniations can be small (for example see panel *B* at 2 o'clock), or appear of a "standard" size (Fig. 4, *A–C*), but not much beyond that even after 9 h at 37°C (*E*). The appearance of the membrane herniations both individually and in clusters along the entire circumference of the nuclear envelope except at points where the nuclear envelope abuts a vacuole (*B*) parallels the reported distribution for nuclear pore complexes in wild-type cells (Severs et al., 1976). We have examined cells from time

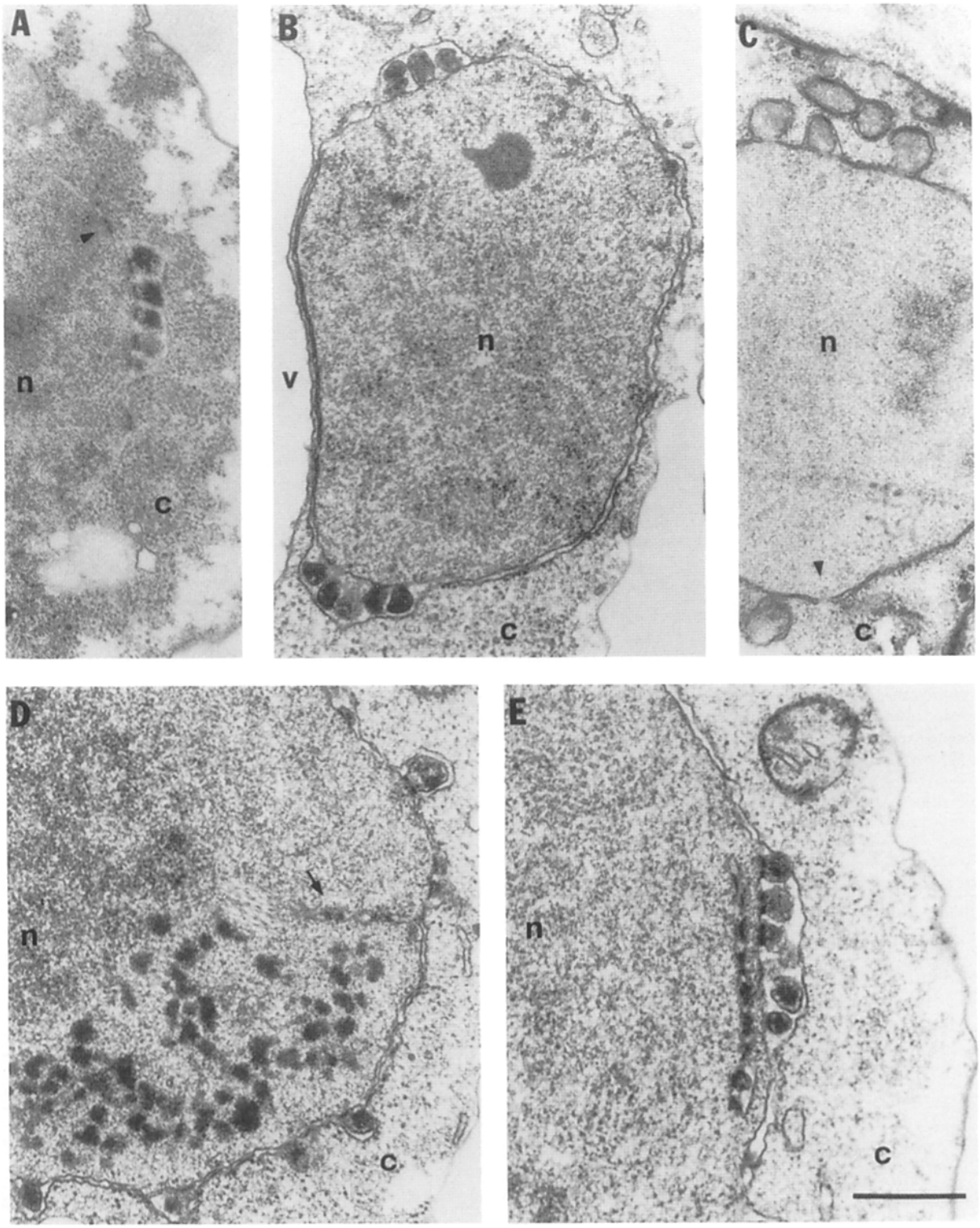

Figure 4. Electron microscopic analysis of the nuclear envelope after growth of *nup116Δ* cells at 37°C. The *nup116Δ* cells (SWY27) were grown to early logarithmic phase at 23°C and then shifted to 37°C for 3 h (*A–D*) or 9 h (*E*) before fixation, embedding, and staining for optimal protein (*A*), membrane (*C*), or protein and membrane (*B, D,* and *E*) visualization (see Materials and Methods). The micrographs show examples of the nuclear membrane herniations, with the electron-dense material inside and the NPC-like structure at their nucleoplasmic base. The arrowheads in *A* and *C* point to examples of apparently unperturbed NPCs and pore membranes, respectively. Note the electron-dense intranuclear material that is of similar density as the material inside the nuclear membrane herniations and was observed only at 37°C (*D*). Inner membrane invaginations as in *D* (*arrow*) and in *E* (at 2 to 4 o'clock) were observed at both the permissive and nonpermissive growth temperatures. *n*, nucleus; *c*, cytoplasm; *v*, vacuole; Bar, 0.5 μm.

points as early as 30 min after the shift to 37°C and we find that the herniations with electron-dense filling are already present (data not shown). Frequently, material of similar electron density can be found intranuclearly (Fig. 4 *D*). To test whether the accumulation of electron dense material in the membrane herniations is dependent upon protein synthesis, *nupl16Δ* cells were shifted to 37°C in either the presence or absence of cycloheximide. We found that cycloheximide has no detectable effect on the nuclear envelope specific phenotype of the *nupl16Δ* cells as the membrane herniations with electron dense filling are still present and structurally identical to those of untreated cells (data not shown). Thus, newly synthesized proteins are not required for formation of the nuclear envelope herniations shown in Figs. 3 and 4.

Fig. 4, *D* (*arrow*) and *E* (from 2 to 4 o'clock) also show invaginations of the inner nuclear membrane that appear to be studded with densities similar in size to NPCs. Similar invaginations are the only observed ultrastructural perturbations when the *nupl16Δ* cells were grown at 23°C (data not shown). Note that unlike the case of nuclear envelope NPCs, there are no apparent herniations at the NPC-like structures of these inner nuclear membrane invaginations, even after growth at 37°C for 9 h (Fig. 4 *E*). All of the above described ultrastructural changes are found in the haploid *nupl16Δ* cells regardless of strain background, as well as in a diploid null strain (SWY59).

Nucleoporins Are Localized at the Base of the Nuclear Envelope Herniations

To determine whether the structures seen at the base of the nuclear membrane herniations (Fig. 4) are NPCs, we used a mixture of the polyspecific MAb192 and MAb350. The specificity of these mAbs for yeast NPCs has been previously established by immunoelectron microscopy (Wente et al., 1992; Rout, M. P., and G. Blobel, personal communication). When *nupl16Δ* cells were shifted for 3 h to 37°C and examined by indirect immunofluorescence microscopy, there was no apparent change in relative intensity and no apparent redistribution in the fluorescence signal. As in wild-type cells, the staining was punctate and limited to the nuclear periphery (data not shown). By immunoelectron microscopy (Fig. 5), gold particles were found at the nucleoplasmic base of the herniations suggesting that the structures found there (Fig. 4) are NPCs that contain at least a subset of nucleoporins. Virtually no gold particles were found inside the compartment formed by the membrane herniation, or on the outer faces of the protrusion (see Table II). Thus, neither site appears to contain MAb192 and MAb350 reactive nucleoporins. Because the morphological preservation in these immunoelectron microscopy samples did not distinguish the inner membrane invaginations, we could not determine whether the densities studding the invaginations contain nucleoporins.

Polyadenylated RNA Accumulates at the Nuclear Periphery

Because NPCs were found at the base of the herniation, and as the accumulation of electron-dense material in the herniation was independent of protein synthesis, it seemed possible that these mutant NPCs may have remained transport competent but that the apparent membrane seal would prevent

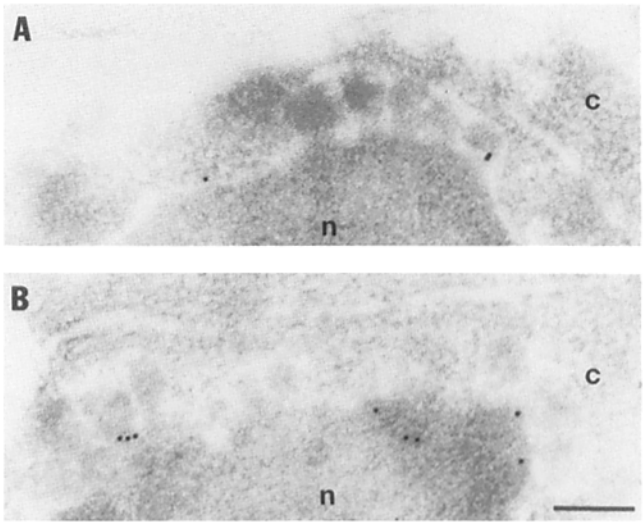

Figure 5. Nucleoporins localize at the base of the nuclear membrane herniations in arrested *nupl16Δ* cells. Immunolabeling with a mixture of MAb192 and MAb350 was performed with thin sections from *nupl16Δ* cells (SWY27) that were grown at 37°C for 3 h before fixing and processing as described in Materials and Methods. In *A* a gold particle along the nuclear envelope to the left of the cluster of protrusions is presumed to be labeling an apparently intact NPC, whereas the two gold particles to the right are at the nucleoplasmic base of the membrane herniations. The tabulation of gold particle localization (Table II) in representative cell thin sections reinforces the conclusions of the two examples presented in *A* and *B*; gold particles preferentially localize only at the base and not within the membrane herniation. Bar, 0.2 μm.

cytoplasmic localization of export substrates. The localization of polyadenylated RNA, an export substrate, was monitored by in situ hybridization with a digoxigenin labeled, oligonucleotide poly(dT)$_{30}$ probe after the shift of *nupl16Δ* cells to growth at 37°C. The signal in *nupl16Δ* cells before the temperature shift is diffuse and cytoplasmic (Fig. 6, *upper left panel*). However, after growth at 37°C for 1 h, the fluorescence signal is predominantly nuclear (Fig. 6, *middle left panel*). This nuclear accumulation is already visible in some *nupl16Δ* cells within 15 min after shifting to 37°C (data not shown). This closely mirrors the time course for the appearance of the nuclear membrane herniations by EM. Interestingly, the staining for polyadenylated RNA was sometimes enhanced in the periphery of the nucleus and was distinctly punctate (see single nucleus in lower third of middle panel of Fig. 6 and the higher magnification view of a single nucleus from a different field in bottom panel of Fig. 6). The peripheral nuclear and distinctly punctate staining was found in at least 20% of the *nupl16Δ* cells grown for 1 h at 37°C. This discrete nuclear localization may reflect not only the inability of polyadenylated RNA to reach the cytoplasm, but also specific accumulation of export substrates within the membrane herniations.

Overexpression of NUP116 Inhibits Cell Growth

Because the absence of *NUP116* had such dramatic effects on cellular growth and nuclear envelope structures, we investigated the effects of overexpressing *NUP116*. The *NUP116*

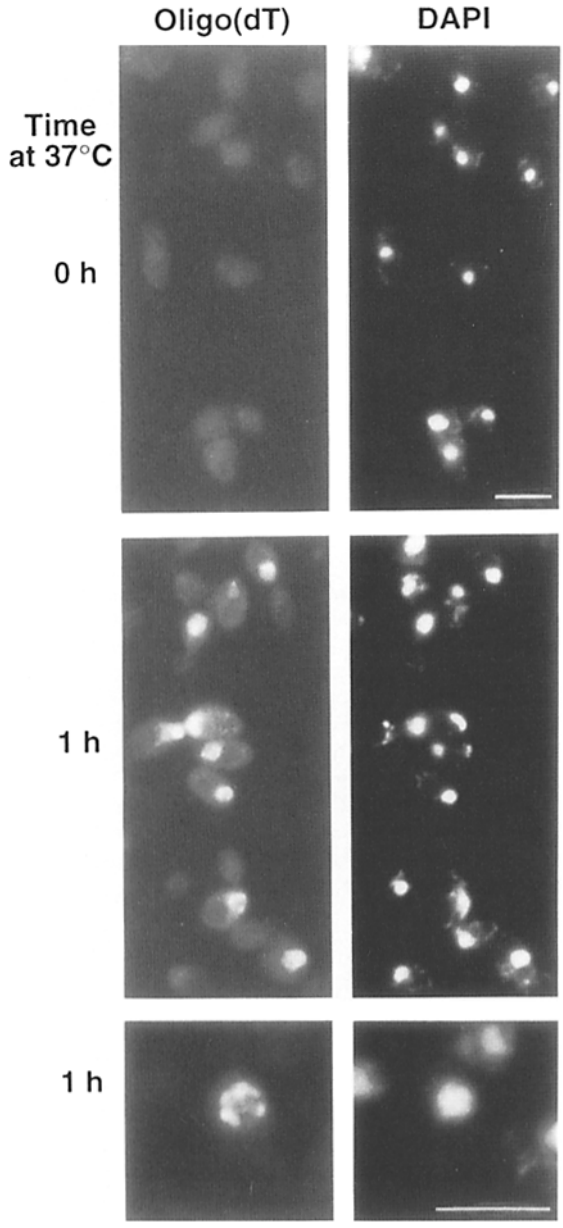

Figure 6. Nuclear accumulation of polyadenylated RNA in *nup116Δ* cells upon the shift to the nonpermissive temperature. *nup116Δ* cells (SWY27) were grown to early logarithmic phase at 23°C in rich media and then shifted to growth at 37°C. Aliquots were removed at the designated time point after the temperature shift, fixed, and processed for in situ hybridization with a digoxigenin-labeled oligonucleotide poly(dT) as described in Materials and Methods. The left panel of photographs shows the fluorescence signal from typical fields of cells that were probed after hybridization with an FITC-conjugated anti-digoxigenin antibody. The right panel is the coincident DAPI staining for the respectively field of cells to the left. The bottom panel is at a higher magnification. By examining the middle panel at various focal planes we found that at least three of the eight staining cells displayed a peripheral nuclear and distinctly punctate pattern similar to the nucleus in the bottom panel (from a different field). All the photographs were taken and printed for the same exposure times. Bar, 6 μm.

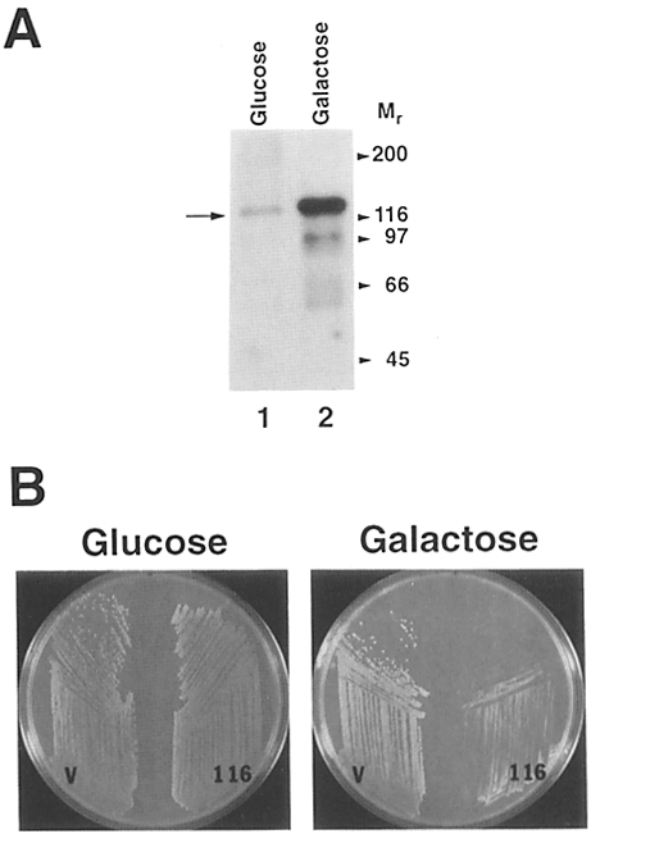

Figure 7. Overexpression of NUP116. (*A*) Immunoblot analysis with MAb192. Yeast strain W303α transformed with pSW134 (SWY-138) was tested for protein expression levels by splitting an early logarithmic phase culture into synthetic defined media lacking uracil (SM-URA) with either 2% glucose or 2% galactose and continuing growth for 8 h at 30°C. Proteins of whole cell extracts from the glucose (lane *1*) and the galactose (lane *2*) cultures were separated by electrophoresis on a 7% SDS polyacrylamide gel, transferred to nitrocellulose, and probed with MAb192 as described in Materials and Methods. The arrow at the left denotes the position of NUP116. Molecular mass markers are indicated at right in kilodaltons. (*B*) Cell growth is severely inhibited upon overexpression of NUP116. Cells from a single colony growing on SM-URA with glucose were streaked onto SM-URA glucose (*left*) and SM-URA galactose (*right*) plates and incubated at 30°C for 48 h. *v*, vector along (pLGSD5); and 116, *GAL10::NUP116* vector (pSW134) transformed into the W303α haploid strain.

gene was placed under the inducible control of the *GAL10* promoter on a 2 μm plasmid (pSW134) and transformed into a wild-type haploid strain. In Fig. 7 *A*, the relative expression level is compared by immunoblot analysis of whole cell extracts from induced and uninduced cultures. Upon induction with galactose (Fig. 7 *A*, lane 2), a considerable overproduction of NUP116 is achieved. The growth in galactose media also dramatically inhibits cell growth (Fig. 7 *B*), such that colony formation is prevented on galactose plates. Microscopic examination of general cellular morphology revealed that cells arrested from overexpression of *NUP116* are the same relative size as cells with the vector alone, and that the overexpressing cells do not arrest synchronously in the cell cycle (data not shown). We also examined the ultrastructure of cells that are overexpressing *NUP116*. In general there

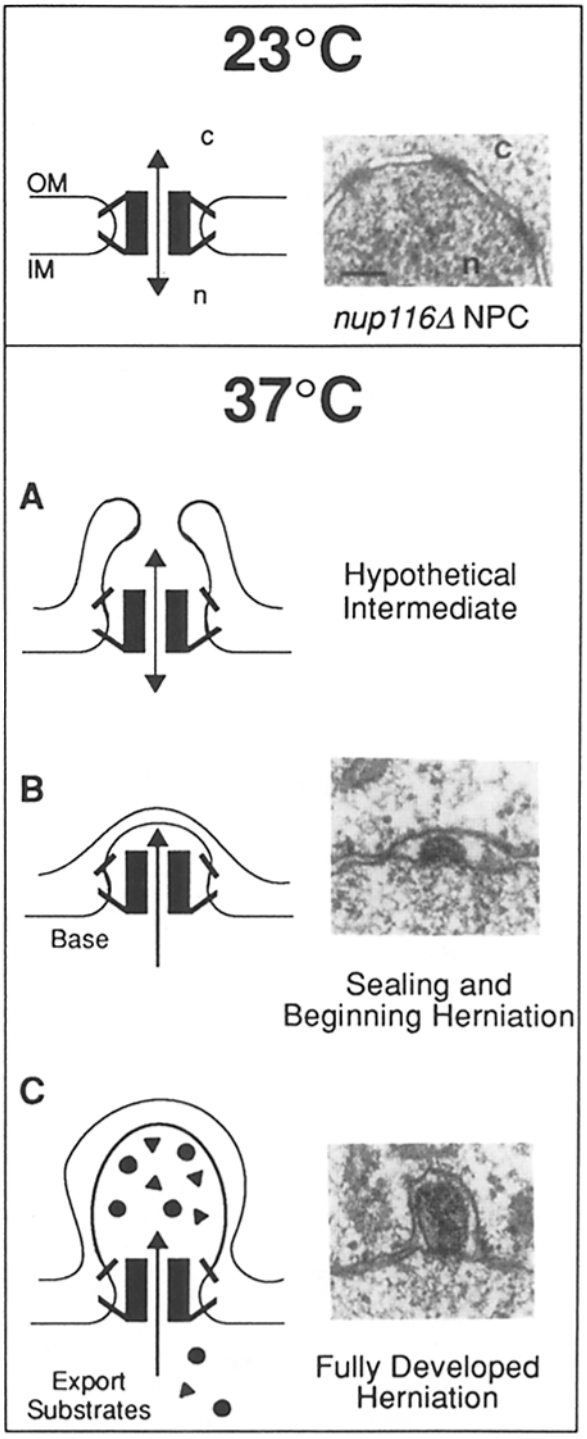

Figure 8. Schematic model for the temperature-induced formation of the *nup116Δ* nuclear envelope herniations. The nuclear envelope associated *nup116Δ* NPCs appear ultrastructurally intact at 23°C (*top panel*). However, when shifted to growth at 37°C a variety of structural perturbations may have occurred. For example, the *nup116Δ* NPCs may undergo a perturbation that weakens the interaction with integral membrane proteins of the pore membrane (*A*). This could then lead to a protrusion of the surrounding membranes and promote nuclear membrane fusion via the hypothetical intermediate (*A*). Membrane fusion across the cytoplasmic face of the NPC effectively seals it and blocks nuclear import (*B*). The continued export of macromolecules through the mutant NPC base structure results in their accumulation in the sealed compartment and the apparent growth of the membrane herniation (*C*). The accompanying panel of typical electron micrographs were selected from *nup116Δ* cells (SWY27) grown at 23°C or at 37°C for 3 h (*B* and *C*) and processed for membrane and protein visualization (see Materials and Methods). All micrographs are at the same magnification and are oriented such that the nucleoplasm at the bottom and the cytoplasm at the top are separated by the nuclear envelope. *IM*, inner nuclear membrane; *OM*, outer nuclear membrane; *c*, cytoplasm; *n*, nucleus; arrows indicate directionality of transport; closed triangles and circles represent "export substrates." Bar, 0.1 μm.

are no noticeable perturbations of nuclear envelope structure, although we find rare occurrences of both inner nuclear envelope invaginations and nuclear envelope herniations. The primary cause of cellular death when *NUP116* is overexpressed requires further investigation.

Discussion

Our data here demonstrate that the absence of a nucleoporin, NUP116, causes highly localized, temperature-sensitive defects in the organization of the nuclear membrane surrounding the NPCs. A double membrane seal is formed over the cytoplasmic side of the mutant NPC at 37°C. This, in turn, prevents nucleocytoplasmic traffic and may thereby contribute to the temperature sensitive lethal phenotype.

These ultrastructural defects are not seen when *nup116Δ* cells are grown at 23°C. Although *nup116Δ* cells grow three times slower than wild-type counterparts at 23°C, the only consistent ultrastructural differences were regularly occurring invaginations of the inner nuclear membrane. These invaginated membranes were studded with densities that resembled NPCs. Such invaginations have not been previously observed in yeast cells, yet they are very similar in structure to the intranuclear annulate lamellae that have been found in other eukaryotic cells (reviewed in Kessel, 1983). The ultrastructure of the nuclear envelope-associated NPCs in *nup116Δ* cells at 23°C appeared to be indistinguishable from that of wild-type cells. The cause of the slower growth rate and the occurrence of the inner nuclear invaginations remains to be investigated. Among several possibilities are diminished rates of NPC assembly and/or diminished rates of nucleocytoplasmic transport by NUP116 deficient NPCs.

When shifted to growth at 37°C, *nup116Δ* cells exhibit a lethal phenotype. Cells are arrested after at most one cellular division and cease being viable thereafter. The ultrastructural changes that were observed are summarized in a highly schematic form in Fig. 8. At 23°C, *nup116Δ* NPCs appear to be ultrastructurally normal and because the cells remain capable of growth and division, these mutant NPCs must be competent for bidirectional nucleocytoplasmic traffic. Within 30 min after shifting to 37°C, a perturbation of the NPC, the pore membrane, and/or the surrounding nuclear envelope occurs. Fig. 8 *A* indicates one of many possibilities, namely that NUP116 deficient NPCs are anchored less tightly to the surrounding pore membrane. This then might allow a protrusion of the adjacent membranes as indicated in Fig. 8 *B*. Such an "intermediate" is likely to be short lived as the protruding membranes would fuse and form a double membrane seal over the cytoplasmic face of the NPC (Fig. 8 *B*). A sealed NPC would no longer allow import to pro-

ceed (Fig. 8 *B*). However, export through the *nup116Δ* NPC might continue to proceed, at least for a while. Accumulation of export substrates on the cytoplasmic side of the sealed NPC could then lead to the observed herniations of the nuclear membrane (Fig. 8 *C*). In addition to export substrates, the herniations may also contain entrapped cytoplasmic components, and/or nucleoporins if the sealed NPCs partially disassemble. However, immunoelectron microscopy analysis with MAb192 and MAb350 showed that at least the nucleoporins recognized by these antibodies are not present within the herniations.

We have shown by in situ hybridization that polyadenylated RNA can be found in discrete punctate patches at the nuclear periphery of *nup116Δ* arrested cells. This is consistent with it being located in the electron-dense material filling the membrane herniation. Definitive localization of the accumulated polyadenylated RNA has to await the development of in situ hybridization methods for yeast cells at the EM level. The intranuclear material of an electron density similar to that found within the nuclear membrane herniations could represent export substrates that accumulate at their sites of transcription or on their way to the NPC. In situ hybridization with oligonucleotide poly(dT) probes has been used to characterize temperature sensitive RNA export mutants (Amberg et al., 1992; Kadowaki et al., 1992). Although mutant alleles of nucleoporins have not yet been reported, our data show that *NUP116* mutants would be isolated by genetic screens of temperature sensitive mutants. However, as proposed here, the defect in the *nup116Δ* cells is not so much a defect in the nuclear export pathway as it is an indirect consequence of membrane sealing over the NPC.

The observed nuclear envelope seal over the cytoplasmic face of the yeast NPC has so far not been reported. It remains to be seen whether this phenomenon represents a general response to defective NPCs, and therefore could occur with a number of nucleoporin mutants, or whether it is limited to mutations in the nucleoporins of the GLFG family or specifically in *NUP116*.

We would like to thank Eleana Sphicas for her expert assistance with the EM studies. We acknowledge the shared advice and reagents of Drs. Philip Bernstein, Charles Cole, Howard Field, and John Heuser. We are also grateful to Drs. Danny Schnell, Susan Smith, Chris Hardy, Mary Moore, and Mike Rout for their helpful discussions and critical reading of the manuscript.

S. R. Wente was supported by a National Research Service Award fellowship (1F32GM14268) for part of this work.

Received 28 May 1993 and in revised form 9 July 1993.

References

Akey, C. W. 1992. The nuclear pore complex: a macromolecular transporter. *In* Nuclear Trafficking. C. Feldherr, editor. Academic Press, New York. 31–70.

Amberg, D. C., A. L. Goldstein, and C. N. Cole. 1992. Isolation and characterization of *RAT1*: an essential gene of *Saccharomyces cerevisiae* required for the efficient nucleocytoplasmic trafficking of mRNA. *Genes & Dev.* 6: 1173–1189.

Bruschi, C. V., A. R. Comer, and G. A. Howe. 1987. Specificity of DNA uptake during whole cell transformation of *S. cerevisiae*. *Yeast.* 3:131–137.

Byers, B., and L. Goetsch. 1991. Preparation of yeast cells for thin-section electron microscopy. *Methods Enzymol.* 194:602–608.

Dabauvalle, M. C., K. Loos, and U. Scheer. 1990. Identification of a soluble precursor complex essential for nuclear pore assembly in vitro. *Chromosoma (Berl.).* 100:56–66.

Davis, L. I., and G. Blobel. 1986. Identification and characterization of a nuclear pore complex protein. *Cell.* 45:699–709.

Davis, L. I., and G. R. Fink. 1990. The *NUP1* gene encodes an essential component of the yeast nuclear pore complex. *Cell.* 61:965–978.

Finlay, D. R., and D. J. Forbes. 1990. Reconstitution of biochemically altered nuclear pores: transport can be eliminated and restored. *Cell.* 60:17–29.

Finlay, D. R., E. Meier, P. Bradley, J. Horecka, and D. J. Forbes. 1991. A complex of nuclear pore proteins required for pore function. *J. Cell Biol.* 114:169–183.

Forbes, D. J. 1992. Structure and function of the nuclear pore complex. *Annu. Rev. Cell Biol.* 8:495–527.

Forrester, W., F. Stutz, M. Rosbash, and M. Wickens. 1992. Defects in mRNA 3′-end formation, transcription initiation, and mRNA transport associated with the yeast mutation prp20: possible coupling of mRNA processing and chromatin structure. *Genes & Dev.* 6:1914–1926.

Franke, W., U. Scheer, G. Krohne, and E. Jarasch. 1981. The nuclear envelope and the architecture of the nuclear periphery. *J. Cell Biol.* 91:39s–50s.

Gerace, L., Y. Ottaviano, and K. C. Kondor. 1982. Identification of a major polypeptide of the nuclear pore complex. *J. Cell Biol.* 95:826–837.

Guarente, L., R. R. Yogum, and P. Gifford. 1982. A *GAL10-CYC1* hybrid yeast promoter identifies the *GAL4* regulatory region as an upstream site. *Proc. Natl. Acad. Sci. USA.* 79:7410–7414.

Hallberg, E., R. Wozniak, and G. Blobel. 1993. An integral membrane protein of the pore membrane domain of the nuclear envelope contains a nucleoporin like region. *J. Cell Biol.* 122:513–521.

Ito, H., Y. Fukuda, K. Murata, and A. Kimura. 1983. Transformation of intact yeast cells treated with alkali cations. *J. Bacteriol.* 153:163–168.

Kadowaki, T., Y. Zhao, and A. M. Tartakoff. 1992. A conditional yeast mutant deficient in mRNA transport from nucleus to cytoplasm. *Proc. Natl. Acad. Sci. USA.* 89:2312–2316.

Kessel, R. G. 1983. The structure and function of annulate lamellae: porous cytoplasmic and intranuclear membranes. *Int. Rev. Cytol.* 82:181–303.

Loeb, J. D. J., L. I. Davis, and G. R. Fink. 1993. *NUP2*, a novel yeast nucleoporin, has functional overlap with other proteins of the nuclear pore complex. *Mol. Biol. Cell.* 4:209–222.

Maul, G. G. 1977. The nuclear and cytoplasmic pore complex: structure, dynamics, distribution, and evolution. *Int. Rev. Cytol. Suppl.* 6:75–186.

Nehrbass, U., H. Kern, A. Mutvei, H. Horstmann, B. Marshallsay, and E. C. Hurt. 1990. NSP1: a yeast nuclear envelope protein localized at the nuclear pores exerts its essential function by its carboxy-terminal domain. *Cell.* 61:979–989.

Radu, A., G. Blobel, and R. W. Wozniak. 1993. Nup115 is a novel nuclear pore complex protein that contains neither repetitive sequence motifs nor reacts with WGA. *J. Cell Biol.* 121:1–9.

Reichelt, R., A. Holzenberg, E. L. Buhle, M. Jarnik, A. Engel, and U. Aebi. 1990. Correlation between structure and mass distribution of the nuclear pore complex and of distinct pore complex components. *J. Cell Biol.* 110:883–894.

Sambrook, J., E. F. Fritsch, and T. Maniatis. 1989. Molecular Cloning: A Laboratory Manual. Cold Spring Harbor Laboratory. Cold Spring Harbor, New York.

Severs, N. J., E. G. Jordan, and D. H. Williamson. 1976. Nuclear pore absence from areas of close association between nucleus and vacuole in synchronous yeast cultures. *J. Ultrastruct. Res.* 54:374–387.

Sheehan, M. A., A. D. Mills, A. M. Sleeman, R. A. Laskey, and J. J. Blow. 1988. Steps in the assembly of replication-competent nuclei in a cell-free system from Xenopus eggs. *J. Cell Biol.* 106:1–12.

Sherman, F., G. R. Fink, and J. B. Hicks. 1986. Methods in Yeast Genetics. Cold Spring Harbor Laboratory, Cold Spring Harbor, New York.

Starr, C. M., M. D'Onofrio, M. K. Park, and J. A. Hanover. 1990. Primary sequence and heterologous expression of nuclear pore glycoprotein p62. *J. Cell Biol.* 110:1861–1871.

Sukegawa, J., and G. Blobel. 1993. A nuclear pore complex protein that contains zinc finger motifs, binds DNA and faces the nucleoplasm. *Cell.* 72:29–38.

Vigers, G. P., and M. J. Lohka. 1991. A distinct vesicle population targets membranes and pore complexes to the nuclear envelope in Xenopus eggs. *J. Cell Biol.* 112:545–556.

Wente, S. R., M. P. Rout, and G. Blobel. 1992. A new family of yeast nuclear pore complex proteins. *J. Cell Biol.* 119:705–723.

Wimmer, C., V. Doye, P. Grandi, U. Nehrbass, and E. C. Hurt. 1992. A new subclass of nucleoporins that functionally interact with nuclear pore protein NSP1. *EMBO (Eur. Mol. Biol. Organ.) J.* 11:5051–5061.

Wozniak, R. W., E. Bartnik, and G. Blobel. 1989. Primary structure analysis of an integral membrane glycoprotein of the nuclear pore. *J. Cell Biol.* 108:2083–2092.

Wright, R., M. Basson, L. DAri, and J. Rine. 1988. Increased amounts of HMG-CoA reductase induce "karmellae": a proliferation of stacked membrane pairs surrounding the yeast nucleus. *J. Cell Biol.* 107:101–114.

Yaffe, M. P., and G. Schatz. 1984. Two nuclear mutations that block mitochondrial protein import. *Proc. Natl. Acad. Sci. USA.* 81:4819–4823.